amcs

COMPARISON OF LINEAR CONTROL METHODS
FOR AN AMB SYSTEM

WOJCIECH GREGA, ADAM PIŁAT

Department of Control, AGH University of Science and Technology
Al. Mickiewicza 30, 30–095 Cracow, Poland
e-mail: {wgr,ap}@ia.agh.edu.pl

The contactless nature of active magnetic bearings brings about many advantages over the conventional bearing while industrial real-time applications are often limited by the significant complexity of control algorithms. This paper presents the application of an LQ controller to an active magnetic bearing system (AMB). Two control strategies are presented and compared: local and global. In the first case the rotor is modelled as two separated masses located at the bearing. In the second case rotor stabilization is considered globally as a problem of the rotating rigid body suspended in a magnetic field. The second approach is especially important for high-speed rotating machines. The control performance of both algorithms was analysed using an experimental AMB laboratory system.

Keywords: active magnetic bearing, real-time control, modelling, LQ control, control performance

1. Introduction

In recent years the number of rotating machines equipped with Active Magnetic Bearings (AMBs) has been increasing. The contactless nature of AMBs brings about many advantages over the conventional bearing such as the elimination of the lubricant medium, less vibration, noise and very high rotational speeds (up to 60 000 RPM) and loads (e.g., 3000 N depending on bearing construction). However, AMBs are not widely applied in industry. Turbo-molecular vacum pumps, flywheel energy storage systems and other high speed rotating machinery are the most significant industrial applications.

One important reason for this is the complexity of the control system. To apply active control to the AMB system, it is necessary to construct a high performance, real-time feedback controller to stabilize and control the suspended rotor. The control design problem is usually quite complicated. This has received much attention in recent years.

The high accuracy in the inherently unstable AMB system necessitates a well-identified mathematical model. The magnetic bearing system is strongly nonlinear due to electromagnetic forces, state and control constraints, and electrical characteristics of the power-supply actuator unit. Those nonlinearities imply that the linear model obtained by local linearization is valid in some region around the operating point. If the operating point moves from the origin position, the system may become unstable due to

neglected nonlinearities (e.g., the tracking problem in the spindle application (Kim *et al.*, 1998)).

In general, for precise control of AMB systems, nonlinear controllers are better than linear ones. The major disadvantage is their complexity and sensitivity. When control computers were slow, it was difficult to apply nonlinear algorithms. Due to fast dynamics of AMB systems, the application of real-time control was always a challenging task. Therefore for AMB systems (Lee and Fan, 1996) a wide range of linear models and controllers were tested and implemented. Some of them approximate the process quite well around the operating point. With the development of today's PC/DSP-based technology, nonlinear methods are more often used in applied AMB control algorithms (Lottin *et al.*, 1996; Piłat, 2000).

The most popular method is feedback linearization used in the control of AMB systems and magnetic suspension systems. It requires the linearity of the system in control inputs. In practice, the feedback linearization algorithm should be combined with other robust control algorithms (Joo and Seo, 1997; Levin *et al.*, 1996; Lin and Gau, 1997) since a mismatch between the model and the process always exists. Therefore, a complete nonlinear robust controller for the AMB, extended by smoothing filters and PWM signal generators, is quite complex and might again create implementation problems.

It is well known that during the implementation phase a control law can be accomplished with different computer realizations. The performance of a control

scheme depends not only on the complexity of the algorithm, but also on the parameters of the computational environment, namely, the sampling period, interrupt latency or the processor word length (Grega, 1997).

Figure 1 illustrates this relation. Depending on computer realization, the assumed control performance can be obtained by a less (A) or a more complex (B) algorithm, while preserving lower computational efforts. The computational effort must take into account not only the number of floating-point operations of the control algorithm, but also another time surplus imposed by the operational system such as task scheduling and data exchange times.
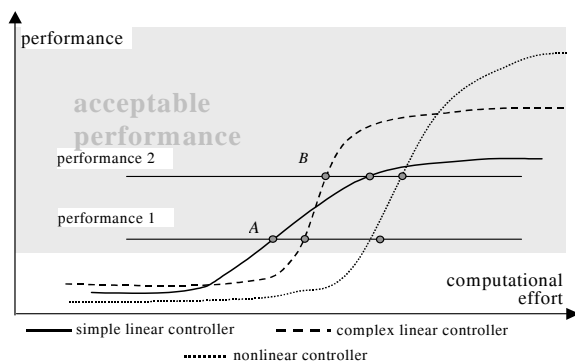
Fig. 1. Control performance and computational effort.

The purpose of this paper is to compare linear control strategies applied to the AMB system. Two aspects are discussed (see Fig. 2). In the first case the rotor is modelled as two separated masses located in the bearings. Thus, only four local controllers are used to stabilize the rotor, one controller for each control axis.

In the second case rotor stabilization is considered globally as a problem of a rotating rigid body suspended in a magnetic field. This is an important case that relates to high-speed rotating machines: the gap between the axis of inertia and the geometric axis of the rotor is responsible for synchronous vibrations of the rotor. The AMB control system can be used to counteract unbalanced behaviour. Mechanical couplings between bearings caused by the rigid body of the rotor are modelled, and interactions between control axis are controlled, using a 16×4 linear controller. This is a more complex, yet comparatively simple controller structure for a computer implementation and, probably, giving a better performance of the control. This aspect was experimentally tested and is described in the final part of the paper.

The system is controlled using a standard PC computer which implements integrated real-time control and rapid prototyping environment. This environment, based on MATLAB/Simulink and the RTWT toolbox, supports automatic generation of the controller code and reveals a
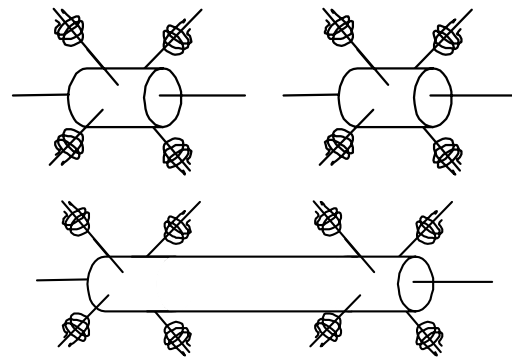
Fig. 2. Two models of the rotor considered in the paper.

real-time performance with small latencies (Mathworks, 1999).

2. System Description

2.1. Experimental Set-Up

The AMB laboratory model (Piłat, 2002) consists of the rotor suspended in two active magnetic bearings. Each bearing is controlled in two perpendicular axes. It is assumed that the rotor is rigid, with its first bending natural frequency higher than the operational speed.
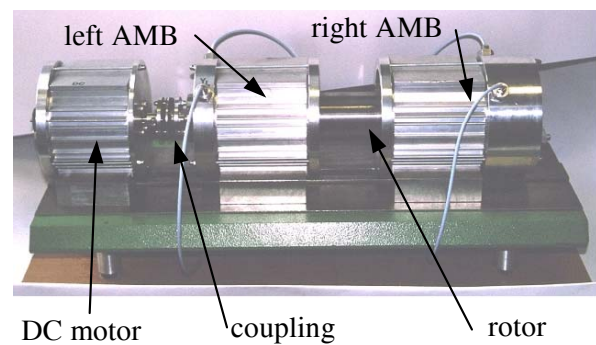
Fig. 3. Active magnetic bearing, laboratory model.

The rotor position is measured by Bently Nevada displacement proximity sensors located at each axis. The electromagnet coils are controlled using a power amplifier with the use of Pulse Width Modulation (PWM). Generally, the system I/O consists of twelve measurements (rotor positions and coil currents) and nine control signals.

The computer-based AMB control system can be classified as time critical in the sense that the sampling rate and performance of the operating system are essential for correct operation of the control system. In many cases the sampling rate is bounded by the parameters of the control computer close to its theoretical minimal value (i.e., given by sampling theory). For this reason contributions of sampling periods and timing delays to the performance

AMB control system are important. The safety margins can be obtained by application of high-speed, but expensive, DSP processors.
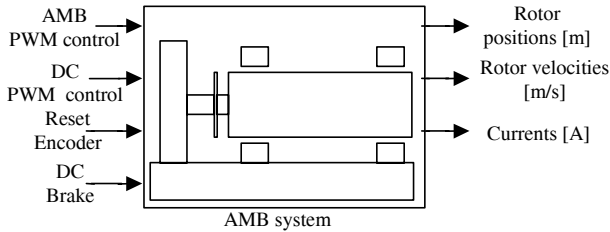

Fig. 4. MATLAB/Simulink interface.

The AMB system block available in Simulink (Fig. 4) contains analogue input, encoder input and PWM output drivers to perform measurements and control. The AMB system was connected to the computer by the RT-DAC3 multi I/O board equipped with an FPGA programmable chip. A user-defined logic dedicated for the AMB system was applied in this case, drastically increasing the control loop throughout and making real-time characteristics of controller compatible with sampling requirements of the process,

2.2. Operation Modes

Three phases can be distinguished during the AMB system operation: rotor levitation (rotor load), rotations of the rotor, rotor unload, c.f. Figs. 5–7.
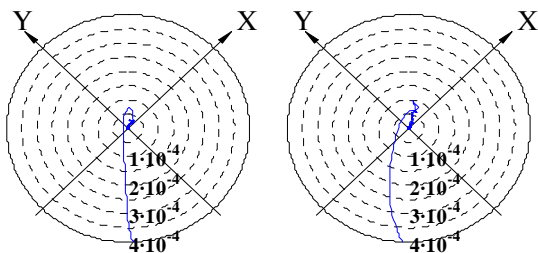

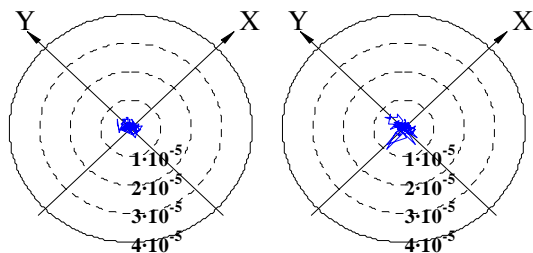Fig. 5. Loading the rotor, the distance between the rotor axis and the bearing centre $[m]$.

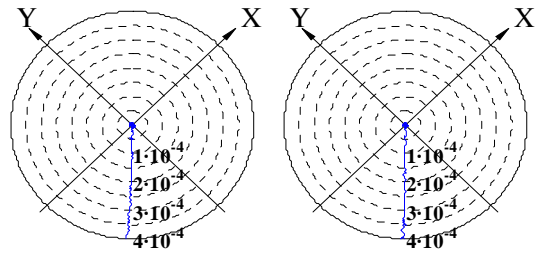Fig. 6. Rotations—rotor stabilization.

Fig. 7. Unloading the rotor.

When the rotor levitates, the control system can realise a number of dedicated algorithms such as stabilisation or trajectory tracking.

3. Local and Global Models of the AMB System

3.1. Local Model

A single magnetic bearing consists of four electromagnets, which can be controlled separately or in pairs. In the configuration considered two pairs of electromagnets are controlled separately. The electromagnets are located at the top and bottom of each axis. Figure 8 presents the configuration of the magnetic bearing and forces acting on the rotor.

It is assumed that the axial configuration of both pairs of electromagnets is identical. Since the axes are perpendicular to each other, a single axis control problem can be analyzed and the results applied to others.
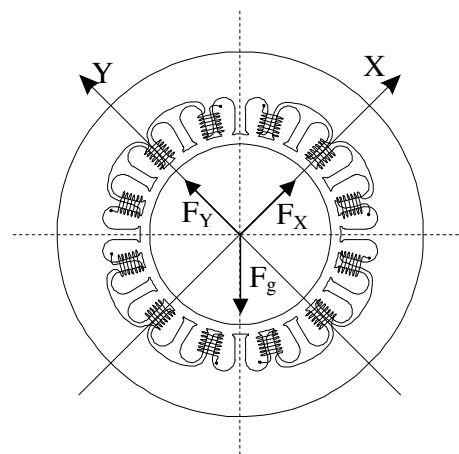

Fig. 8. Configuration of the rotor in the AMB system.

For active magnetic bearings the electromagnetic force can be calculated according to the standard model published previously in several books and conference pa-

pers (Maslen, 1995; Schweitzer *et al.*, 1994):

$$F_{\mathrm{up}} = \frac{1}{2} K \frac{x_3^2}{x_1^2}, \qquad (1)$$

where x_1 is the axial rotor position, K is an electromagnet constant and x_3 denotes the current in the coil.

The electromagnetic force model (Piłat, 2002) applied in this paper is based on the following dependence of coil inductance on the rotor distance from the electromagnet surface:

$$L'(x_1) = \frac{\mathrm{d}L(x_1)}{\mathrm{d}x_1} = -\frac{L_0}{b} \exp\left(\frac{-x_1}{b}\right) + 2cx_1, \qquad (2)$$

where L_0 means the coil inductance for rotor located at the electromagnet (the distance equal to zero), b and c are constants, and x_1 stands for the axial rotor position.
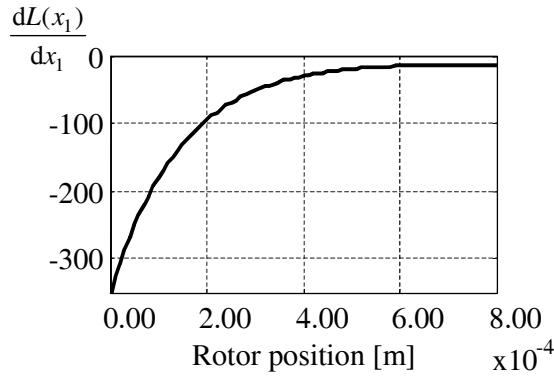

Fig. 9. Coil inductance vs. the rotor position.

Identification experiments (Piłat, 2002) demonstrated that for the analysed active magnetic bearing the model (2) gives a better representation than the standard one (1) due to the electromagnet construction and the air gap size.

Therefore, the forces generated by upper and lower electromagnets are given as follows:

$$F_{\mathrm{up}} = \frac{1}{2} L'(x_1) x_3^2, \quad F_{\mathrm{bottom}} = \frac{1}{2} L'(d - x_1) x_4^2. \quad (3)$$

The electromagnetic force acting on the suspended mass is calculated as a sum of electromagnetic forces produced by the lower and upper electromagnets along the axis considered. The electromechanical model for the single axis is given by

$$\begin{cases} \dot{x}_1 = x_2, \\ \dot{x}_2 = \dfrac{1}{2m}\left[L'(x_1)\cdot x_3^2 - L'(d - x_1)\cdot x_4^2\right] + \dfrac{F_{gX}}{m}, \\ \dot{x}_3 = \dfrac{a_3(u_{c3} - u) + b_3 - P1_3 x_3}{P2_3}, \\ \dot{x}_4 = \dfrac{a_4(u_{c4} + u) + b_4 - P1_4 x_4}{P2_4}, \end{cases} \qquad (4)$$

where we use the following notation:

x_1 axial mass position [m],

x_2 axial mass velocity [m/s],

x_3 upper coil current of the analysed control axis [A],

x_4 lower coil current of the analysed control axis [A],

u control signal, PWM duty,

u_{c3} constant control value of the upper coil,

u_{c4} constant control value of the lower coil,

m mass suspended in the bearing [kg],

d maximum air gap [m],

$F_{gX} = F_{gY}$ gravitation force acting in the control axis [N],

$L(x_1)$ coil inductance [H],

$a_i, b_i, P1_i, P2_i$ actuator parameters, $i = \{3, 4\}$.

The control signal applied to the lower electromagnet and the control signal applied to the upper one differ only by their signs, so the control method is referred to as a difference one. States and control signals are bounded as follows:

$$x_1 \in [0, d], \quad x_2 \in \mathbb{R}, \quad x_3 \in [0, 5], \quad x_4 \in [0, 5],$$

$$(u_{c3} - u) \in [0, 1], \quad (u_{c4} + u) \in [0, 1].$$

Constant control values depend on the steady-state current value chosen for the selected operating point. Magnetic bearing stiffness can be adjusted by choosing the appropriate value of coil currents. The actuator controls the current in the coils, and thus the electrical equations (4) are modelled without any influence of the coil inductance.

Most system parameters were obtained using identification procedures (Piłat, 2002). The parameters of the dynamical equations for coil currents were identified separately. Then the electromagnetic force parameters were identified by means of the measured current and position signals. For this identification procedure a step response experiment in a closed loop was performed.

For the operating point of the rotor located at the bearing centre, the electromagnetic force characteristics were calculated as functions of the rotor position and coil current. Figures 10 and 11 reveal that there is a high force sensitivity to deviations from the selected operating point.

Standard linearization, valid in some neighbourhood of the operating point, gives the following local model:

$$\begin{cases} \Delta \dot{x} = J \Delta x + B \Delta u, \\ \Delta y = C \Delta x, \end{cases} \qquad (5)$$
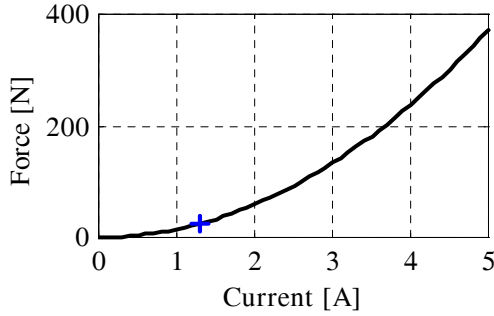
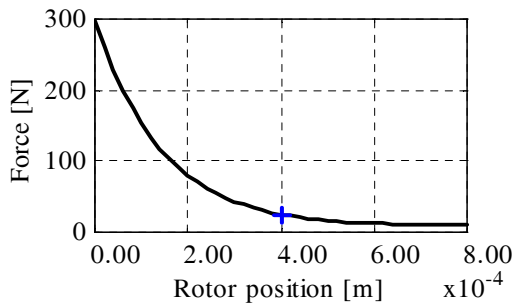Fig. 10. Force vs. current for a fixed rotor position.

Fig. 11. Force vs. the rotor position for a fixed value of the current.

where

$$J = \begin{bmatrix} 0 & 1 & 0 & 0 \\ J_{2,1} & 0 & J_{2,3} & J_{2,4} \\ 0 & 0 & J_{3,3} & 0 \\ 0 & 0 & 0 & J_{4,4} \end{bmatrix}, \quad B = \begin{bmatrix} 0 \\ 0 \\ B_3 \\ B_4 \end{bmatrix},$$

$$J_{2,1} = \frac{1}{2m} \left[L''(\bar{x}_1) x_{30}^2 + L''(d - \bar{x}_1) \bar{x}_4^2 \right],$$

$$J_{2,3} = \frac{\bar{x}_3}{m} L'(\bar{x}_1), \quad J_{2,4} = -\frac{\bar{x}_4}{m} L'(d - \bar{x}_1),$$

$$J_{3,3} = -\frac{P1_3}{P2_3},$$

$$J_{4,4} = -\frac{P1_4}{P2_4}, \quad B_3 = -\frac{a_3}{P2_3}, \quad B_4 = \frac{a_4}{P2_4},$$

$$C = \begin{bmatrix} 1 & 0 & 1 & 1 \end{bmatrix}.$$

3.2. Global Model

In this case the rotor suspended by two AMBs is considered. The rotor position in the XYZ-co-ordinates is presented in Fig. 12. For this model the couplings caused by the rigid body of the rotor are modelled.
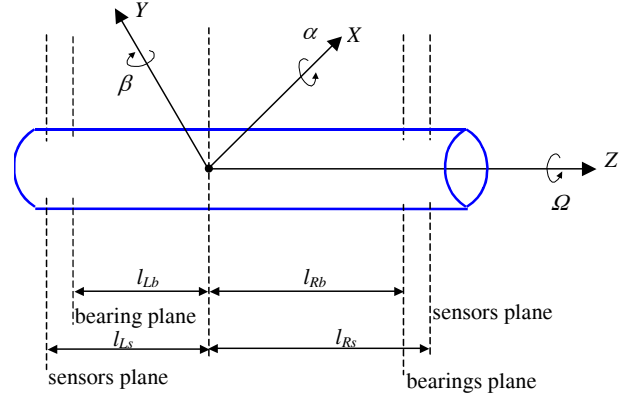

Fig. 12. Full model of the rotor.

Due to mechanical couplings, the axial movement in the Z direction is neglected. Any movement of the rotor inside its AMBs can be represented as a combination of a translation movement and a tilting one. Mechanical equations describing the rotor movement at the bearings middle planes (Gosiewski, 1999; Piłat, 2002) are as follows:

$$\ddot{q}_b = -\Omega I_Z \begin{bmatrix} 0 & T_b M^{-1} G T_b^{-1} \\ -T_b M^{-1} G T_b^{-1} & 0 \end{bmatrix} \dot{q}_b$$

$$+ \begin{bmatrix} T_b M^{-1} T_b^T & 0 \\ 0 & T_b M^{-1} T_b^T \end{bmatrix} F \qquad (6)$$

$$- \begin{bmatrix} T_b M^{-1} N & 0 \\ 0 & T_b M^{-1} N \end{bmatrix} Q,$$

where we use the following notatation:

$q_b = \begin{bmatrix} x_{Lb} & x_{Rb} & y_{Lb} & y_{Rb} \end{bmatrix}^T$
co-ordinates at bearings planes,

$F = \begin{bmatrix} F_{LX} & F_{RX} & F_{LY} & F_{RY} \end{bmatrix}^T$
forces at bearings planes,

$Q = \begin{bmatrix} Q_X & 0 & Q_Y & 0 \end{bmatrix}^T$
gravitation force acting at the mass centre,

$M = \begin{bmatrix} m & 0 \\ 0 & I_x \end{bmatrix}, \quad G = \begin{bmatrix} 0 & 0 \\ 0 & 1 \end{bmatrix},$

$N = \begin{bmatrix} 1 & 0 \\ 0 & 0 \end{bmatrix}, \quad T_b = \begin{bmatrix} 1 & -l_{Lb} \\ 1 & l_{Rb} \end{bmatrix}$
transformation matrix of co-ordinates,

I_X moment of inertia around the axis X ($I_X = I_Y$),

I_Z moment of inertia around the axis Z,

Ω rotational velocity.

The electromagnetic forces acting on the rotor in all four axes are respectively described by the third and fourth equations of the model (4). The mechanical equations (6) are extended by eight electrical equations.

Finally, the linear model obtained by linearization at the operating point is described by (5). Equations given in this form consider solid body couplings. In the global case, the elements of the matrix J given in the general form (5) are

$$J_{1,5} = 1, \quad J_{2,6} = 1, \quad J_{3,7} = 1, \quad J_{4,8} = 1,$$

$$J_{5,1} = h_1 \left[\frac{1}{2} L'' \left(x_c - \bar{x}_1 \right) \bar{x}_9^2 + \frac{1}{2} L'' \left(x_c + \bar{x}_1 \right) \bar{x}_{10}^2 \right],$$

$$J_{5,2} = h_2 \left[\frac{1}{2} L'' \left(x_c - \bar{x}_2 \right) \bar{x}_{11}^2 + \frac{1}{2} L'' \left(x_c + \bar{x}_2 \right) \bar{x}_{12}^2 \right],$$

$$J_{5,7} = -h_4 l_{Lb}, J_{5,8} = h_4 l_{Lb},$$

$$J_{5,9} = -h_1 L' \left(x_c - \bar{x}_1 \right) \bar{x}_9,$$

$$J_{5,10} = h_1 L' \left(x_c + \bar{x}_1 \right) \bar{x}_{10},$$

$$J_{5,11} = -h_2 L' \left(x_c - \bar{x}_2 \right) \bar{x}_{11},$$

$$J_{5,12} = h_2 L' \left(x_c + \bar{x}_2 \right) \bar{x}_{12},$$

$$J_{6,1} = h_2 \left[\frac{1}{2} L'' \left(x_c - \bar{x}_1 \right) \bar{x}_9^2 + \frac{1}{2} L'' \left(x_c + \bar{x}_1 \right) \bar{x}_{10}^2 \right],$$

$$J_{6,2} = h_3 \left[\frac{1}{2} L'' \left(x_c - \bar{x}_2 \right) \bar{x}_{11}^2 + \frac{1}{2} L'' \left(x_c + \bar{x}_2 \right) \bar{x}_{12}^2 \right],$$

$$J_{6,7} = h_4 l_{Rb}, J_{6,8} = -h_4 l_{Rb},$$

$$J_{6,9} = -h_2 L' \left(x_c - \bar{x}_1 \right) \bar{x}_9,$$

$$J_{6,10} = h_2 L' \left(x_c + \bar{x}_1 \right) \bar{x}_{10},$$

$$J_{6,11} = -h_3 L' \left(x_c - \bar{x}_2 \right) \bar{x}_{11},$$

$$J_{6,12} = h_3 L' \left(x_c + \bar{x}_2 \right) \bar{x}_{12},$$

$$J_{7,3} = h_1 \left[\frac{1}{2} L'' \left(x_c - \bar{x}_3 \right) \bar{x}_{13}^2 + \frac{1}{2} L'' \left(x_c + \bar{x}_3 \right) \bar{x}_{14}^2 \right],$$

$$J_{7,4} = h_2 \left[\frac{1}{2} L'' \left(x_c - \bar{x}_4 \right) \bar{x}_{15}^2 + \frac{1}{2} L'' \left(x_c + \bar{x}_4 \right) \bar{x}_{16}^2 \right],$$

$$J_{7,5} = h_4 l_{Lb}, \quad J_{7,6} = -h_4 l_{Lb},$$

$$J_{7,13} = -h_1 L' \left(x_c - \bar{x}_3 \right) \bar{x}_{13},$$

$$J_{7,14} = h_1 L' \left(x_c + \bar{x}_3 \right) \bar{x}_{14},$$

$$J_{7,15} = -h_2 L' \left(x_c - \bar{x}_4 \right) \bar{x}_{15},$$

$$J_{7,16} = h_2 L' \left(x_c + \bar{x}_4 \right) \bar{x}_{16},$$

$$J_{8,3} = h_2 \left[\frac{1}{2} L'' \left(x_c - \bar{x}_3 \right) \bar{x}_{13}^2 + \frac{1}{2} L'' \left(x_c + \bar{x}_3 \right) \bar{x}_{14}^2 \right],$$

$$J_{8,4} = h_3 \left[\frac{1}{2} L'' \left(x_c - \bar{x}_4 \right) \bar{x}_{15}^2 + \frac{1}{2} L'' \left(x_c + \bar{x}_4 \right) \bar{x}_{16}^2 \right],$$

$$J_{8,5} = -h_4 l_{Rb}, \quad J_{8,6} = h_4 l_{Rb},$$

$$J_{8,13} = -h_2 L' \left(x_c - \bar{x}_3 \right) \bar{x}_{13},$$

$$J_{8,14} = h_2 L' \left(x_c + \bar{x}_3 \right) \bar{x}_{14},$$

$$J_{8,15} = -h_3 L' \left(x_c - \bar{x}_4 \right) \bar{x}_{15},$$

$$J_{8,16} = h_3 L' \left(x_c + \bar{x}_4 \right) \bar{x}_{16},$$

$$J_{9,9} = -\frac{P1_9}{P2_9}, \quad J_{10,10} = -\frac{P1_{10}}{P2_{10}}, \quad J_{11,11} = -\frac{P1_{11}}{P2_{11}},$$

$$J_{12,12} = -\frac{P1_{12}}{P2_{12}}, \quad J_{13,13} = -\frac{P1_{13}}{P2_{13}}, \quad J_{14,14} = -\frac{P1_{14}}{P2_{14}},$$

$$J_{15,15} = -\frac{P1_{15}}{P2_{15}}, \quad J_{16,16} = -\frac{P1_{16}}{P2_{16}}.$$

Other elements of the matrix J are zero. The non-zero elements of the matrix B are

$$B_{9,1} = -\frac{a_9}{P2_9}, \qquad B_{10,1} = \frac{a_{10}}{P2_{10}},$$

$$B_{11,2} = -\frac{a_{11}}{P2_{11}}, \qquad B_{12,2} = \frac{a_{12}}{P2_{12}},$$

$$B_{13,3} = -\frac{a_{13}}{P2_{13}}, \qquad B_{14,3} = \frac{a_{14}}{P2_{14}},$$

$$B_{15,4} = -\frac{a_{15}}{P2_{15}}, \qquad B_{16,4} = \frac{a_{16}}{P2_{16}},$$

$$C = \begin{bmatrix} 1 & 1 & 1 & 1 & 0 & 0 & 0 & 0 & 1 & 1 & 1 & 1 & 1 & 1 & 1 & 1 \end{bmatrix},$$

where we adopt the following notation:
$x_1, \ldots, x_4$ axial mass positions in the axes LX, PX, LY, PY, respectively,
$x_5, \ldots, x_8$ axial mass velocities in the axes LX, PX, LY, PY, respectively,
d bearing slackness (air gap),
x_c rotor location at the bearing centre, $x_c = d/2$,
$F_{gX} = F_{gY}$ gravitation force,
$L(\cdot)$ coil inductance,
$a_i, b_i, P1_i, P2_i$ actuator parameters, $i = \{9, \ldots, 16\}$,
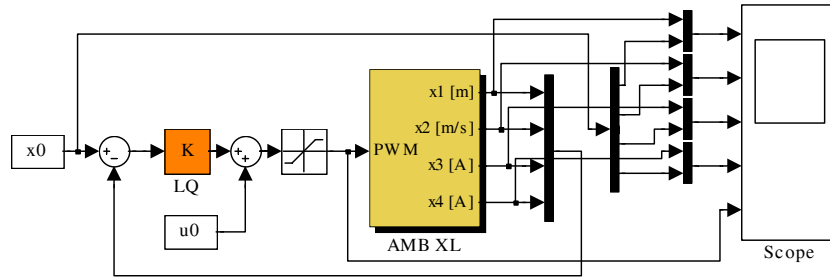
Fig. 13. MATLAB/Simulink local LQ controller loop for a single axis.

$$h_1 = \frac{1}{m} + \frac{1}{I_X} l_{Lb}^2, \quad h_2 = \frac{1}{m} - \frac{1}{I_X} l_{Lb} l_{Pb},$$

$$h_3 = \frac{1}{m} + \frac{1}{I_X} l_{Pb}^2, \quad h_4 = \frac{\Omega I_Z}{(l_{Lb} + l_{Pb}) I_X}.$$

Moreover, the constraints are given as

$$x_i \in [-d/2, d/2] \text{ for } i = \{1, \ldots, 4\}, \ x_2 \in \mathbb{R},$$

$$x_i \in [0, 5], \quad i = \{9, \ldots, 16\}.$$

4. LQ Controller Design

To compare the performance of the controllers developed according to local and global models, LQ controllers were designed. A typical optimization criterion (Mitkowski, 1991) was used, i.e.,

$$J(u) = \frac{1}{2} \int_0^\infty \left[e^T(\tau) Q e(\tau) + u^T(\tau) R u(\tau) \right] \mathrm{d}\tau,$$

where $e(\tau) = x_0 - x(\tau)$, $Q^T = Q \geq 0$, $R^T = R > 0$.

For the models (4) and (6) the `lqr` procedure from the *Matlab Control System Toolbox* was applied for solving the associated matrix Riccati equations, finally producing optimal gains of the linear controllers.

4.1. Local Controller

The simplified model described by (4) treats the rotor as a system of separated masses located in bearings. Since the rotor is asymmetrically suspended in four active magnetic bearings, the problem under consideration is the control of different masses located at the separate bearings.

In the case of separate models, four local LQ optimal controllers were obtained, one controller for each control axis.

The weighting matrices were selected by choosing Q to be diagonal of the rank 4 with all diagonal elements positive and R scalar. For the selected operating point we

get $x_0 = \mathrm{col} \left(4.0 \cdot 10^{-4}, 0, 1.5047, 0.8 \right)$, $u_0 = 0$, $u_{c3} = 0.3533$, $u_{c4} = 0.2656$, and the controller parameters were as follows:

$$K = \left[\begin{array}{cccc} 9.8499 \times 10^2, & 4.0054, & -7.5880 \times 10^{-2}, \\ & & 6.163 \times 10^{-2} \end{array} \right]$$

for $Q = \mathrm{diag} \left(1 \times 10^4, 1 \times 10^{-4}, 1 \times 10^{-4}, 1 \times 10^{-4} \right)$ and $R = 1$, and set as constant for every rotational velocity.

4.2. Global Controller

In the case of the global model, a single controller $K_{16 \times 4}$ was designed. From (5) it follows that the coefficients of this controller depend on the rotational velocity Ω.

The global controller gain matrix is

$$K = \begin{bmatrix} K_{1,1} & K_{1,2} & K_{1,3} & 0 & K_{1,5} & K_{1,6} & 0 & 0 \\ K_{2,1} & K_{2,2} & 0 & K_{2,4} & 0 & 0 & K_{2,7} & K_{2,8} \end{bmatrix}. \tag{7}$$

Its elements are 2×2 matrices. When the rotational velocity is set to zero ($\Omega = 0$), the elements $K_{1,2}$ and $K_{2,1}$ are also zero.

5. System Parameters

The measurements of physical parameters of the AMB laboratory model and the results of identification procedures are summarized in Table 1.

Actuator unit parameters are characterized by the coefficients a_i, b_i, $P1_i$ and $P2_i$. The mechanical construction of the system allows us to calculate the masses suspended in both bearings.

6. Model Comparison

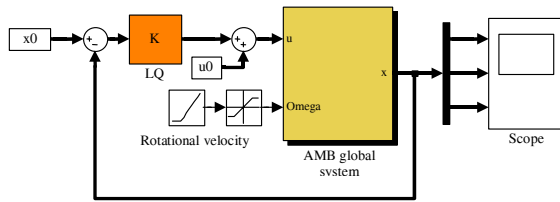To compare the behaviour of the AMB system controlled by local and global controllers, simulation and real-time

Fig. 14. MATLAB/Simulink global LQ controller loop.

Table 1. Selected AMB system parameters.

Parameter	Value
m	7.335 [kg]
m_{bL}	3.667 [kg]
m_{bP}	3.668 [kg]
g	9.81 [m/s^2]
l	0.359 [m]
r	0.02845 [m]
l_{Lcz}	0.1595 [m]
l_{Lb}	0.1006 [m]
l_{Pcz}	0.1655 [m]
l_{Pb}	0.1005 [m]
d	8×10^{-4} [m]
x_c	4×10^{-4} [m]
I_X	2.6204×10^{-4} [kgm^2]
I_Z	2.6204×10^{-4} [kgm^2]
L_0	5.2301×10^{-2} [H]
b	1.4897×10^{-4} [m]
c	-7.2187×10^3 [H/m^2]
d	8.0×10^{-4} [m]
a_3	8.44714 [A]
a_4	8.39955 [A]
b_3	1.56498 [A]
b_4	1.66871 [A]
$P1_3$	0.802956
$P1_4$	0.799153
$P2_3$	0.002512 [s]
$P2_4$	0.002322 [s]

experiments were performed. The local and global control loop schemes developed in the Simulink environment are presented in Figs. 13 and 14.

The development of the real-time application was automated due to code generation capabilities of the MATLAB/RTWT environment. Once the simulation model was completed, an appropriate input/output driver (Fig. 4) was added to generate an executable code directly from the block diagram. From the designer's point of view, it was the same conceptual controller model representation during the design and real-time implementation phases.

The desired rotor position was changed for the right bearing by $\pm 3.0 \cdot 10^{-5}$ m in both axes in order to observe the vertical rotor movement. The left rotor was stabilized at the bearing centre. Time responses of the model and real system are presented in Figs. 15–17.
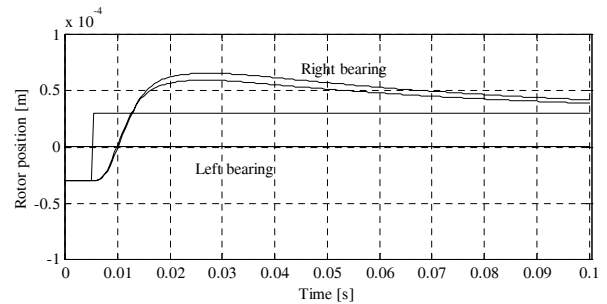

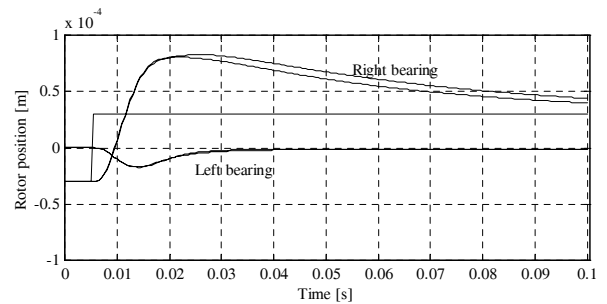Fig. 15. Rotor positions—the local model (simulation).

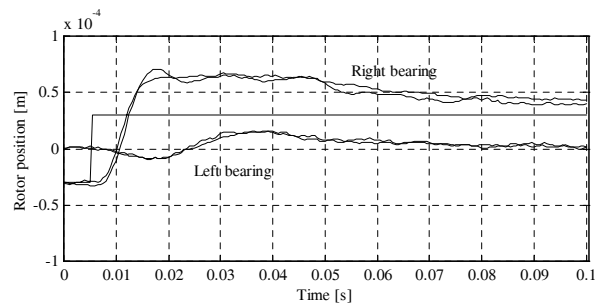Fig. 16. Rotor positions—the global model (simulation).

Fig. 17. Rotor positions–an experiment (the global model).

Figures 15 and 16 show that both controllers exhibit proper behaviour. In both cases the controllers stabilize the rotor at the bearing centre. Figure 17 depicts a typical problem that occurs when a well-tuned controller from a simulation is applied to a real process. Due to disturbances and a mismatch between the simulation model and the process, undesired oscillations appear.

7. Testing Controllers

During the experiments the maximal values of the rotor displacement from the bearing centre were recorded. To investigate the performance of the applied controller for the levitated and rotated rotor, the criterion

$$J = \sqrt{(x_M - x_O)^2 + (y_M - y_O)^2} \qquad (8)$$

for

$$x_M = \max_{t>0}\big(x(t)\big), \quad y_M = \max_{t>0}\big(y(t)\big),$$

was proposed, where x_M and y_M are the axial rotor co-ordinates of the maximum rotor displacements from the bearing centre (x_0, y_0).

A smaller value of the performance criterion (8) confirms higher insensitivity of the control algorithm to disturbances.

The stabilization at the bearing centre was applied and the rotational velocity was set to 550 rpm. The results of the experiment when the local control algorithm was applied are presented in Fig. 18.
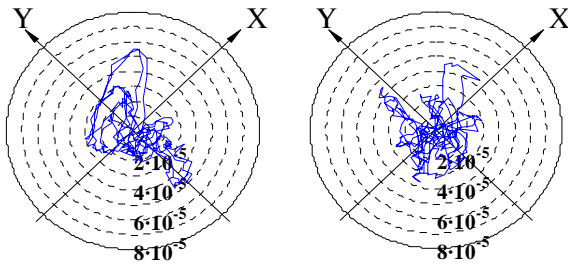

Fig. 18. Trajectory of the rotor position in left and right bearings.

Table 2. Experimental results—the local controller.

Bearing	J
left	5.5242×10^{-5}
right	4.4425×10^{-5}

In the next experiment, a global controller was used. The coefficients of the LQ controller were calculated for the zero rotational velocity ($\Omega = 0$). Then the control algorithm was tested at the speed $\Omega = 550$ rpm. The results are presented in Fig. 19 and Table 3.

Table 3. Experimental results—the global controller.

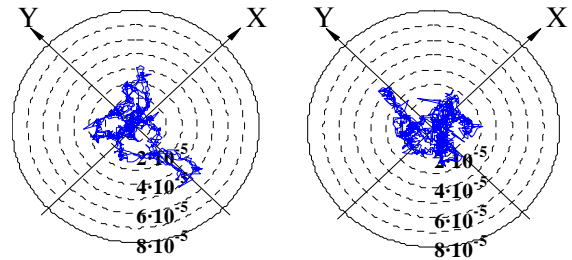| Bearing	J
left	5.3501×10^{-5}
right	4.2831×10^{-5}

Fig. 19. Trajectory of the rotor position in left and right bearings.

To estimate the influence of the rotational velocity on the LQ controller, the parameters of the controller were calculated once again with the same value of Q, and R but for the desired value of $\Omega = 550$ rpm. The results of the experiment are presented in Fig. 20 and Tab. 4.
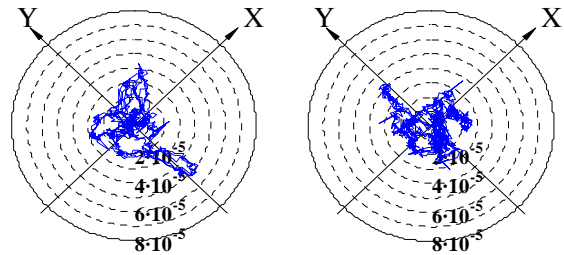

Fig. 20. Trajectory of the rotor position in left and right bearings.

Table 4. Experimental results—the global controller.

Bearing	J
left	5.2175×10^{-5}
right	4.2701×10^{-5}

The experimental results confirm the expected property of the global model: the introduced couplings allow us to compensate for the effects of the total rotor movement. The best results can be achieved using the global control algorithm tuned for the desired rotational velocity.

8. Simulation of a Change in the Rotational Speed

The behaviour of the rotor suspended in two AMBs can be analyzed at the desired value of the rotational speed. The simulation of a global model can provide important information about controller sensitivity. To this end, the global LQ controller gain matrix was calculated for three cases: a low rotational speed, a high rotational speed and each desired rotational speed. Next, the control system

was tested while the rotational speed was changed with the same rate. Figures 21–23 present the location of four dominant eigenvalues of the closed-loop system related to the rotor position.
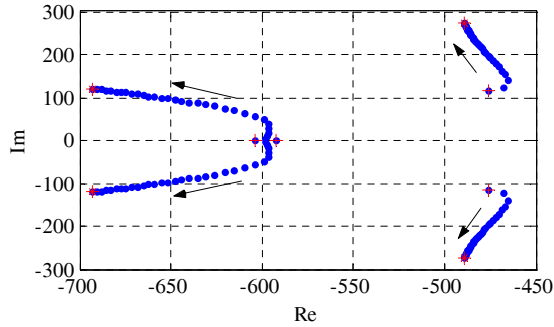

Fig. 21. Root location for the closed-loop system with the LQ controller designed for $\Omega = 0$ and increased to 30 000 1/s (simulation).
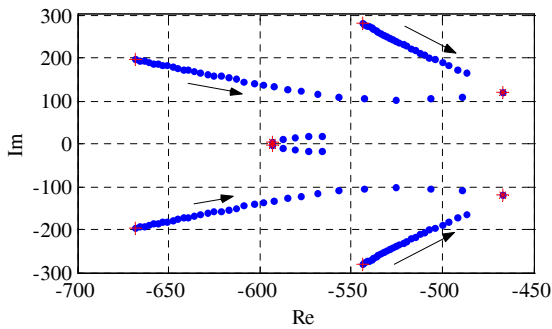

Fig. 22. Root location for the closed-loop system with the LQ controller designed for $\Omega = 30\,000$ 1/s and decreased to 0.
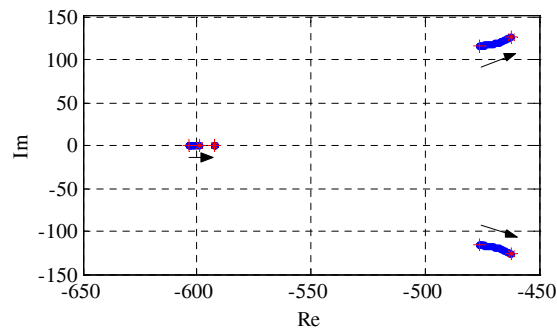

Fig. 23. Root location for the closed-loop system with LQ controller parameters adapted for each rotational velocity, $\Omega \in [30000, 0]$.

Simulation results show that the controller should be designed separately for each rotational speed. Thus an adaptive or a fuzzy logic controller can be appropriate in this case.

9. Estimation of the Computational Effort

The computational effort depends on the controller configuration. Three parameters were calculated for each class of the controllers: the number of multiplications, additions and measurements. The results are presented in Fig. 24.
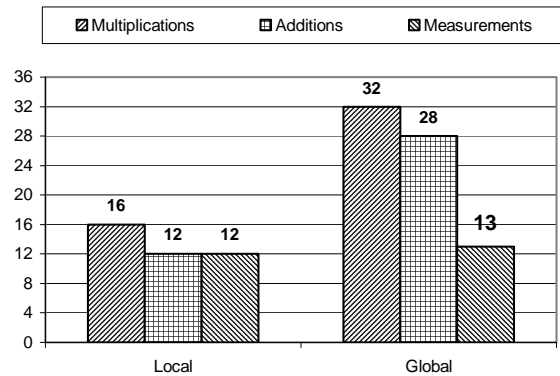

Fig. 24. Computational effort: comparison of local and global controllers.

In the case of the global controller, the number of measurements increases due to the dependence of rotations. For the global controller the number of computations is greater than that in the local one due to the dimension of the controller, which is rather clear.

Table 5 gives a summary of the recorded execution times representing a real-time implementation of the models. The task time given in the table is the total time of analog/digital conversion, system scheduling, data exchange and control signal computations.

Table 5. Task times.

Controller	Task time [μs]
local	283.0327
global	282.1750

The task time of the local controllers is longer than the time recorded for the global controller. It is due to a greater number of subsystems and signal lines used in real time by local controllers. As far as a real-time code implementation is concerned, memory allocation for arrays is more effective than for a number of separate variables. Therefore, the increase in the number of operations required for signal calculation of the global controller was compensated for using a more effective structure of the real-time code, finally giving a decrease in the task time.

10. Conclusion

Two model-based control methods of the AMB system were proposed and tested using simulations and real-time experiments. The application of a more complex mathematical model results in a better control performance. The expected properties of the global model were confirmed: the introduced cross-couplings in the global model are able to compensate for the effects of synchronous vibrations of the rotor by the action of a full-order controller. It was demonstrated that the AMB control system implementing the global controller shows a better performance under a lower computational effort. The controller parameters obtained for the global model are sensitive to rotor velocity. This suggests the application of the gain scheduling method to the adaptation of controller parameters for a higher range of rotation speeds. The proposed multi-dimensional, crosscoupled 16×4 structure of the linear controller is comparatively simple for a computer implementation. The related real-time application can be executed in a shorter time than the control algorithm corresponding to the local models.

References

Gosiewski Z. (1999): *Magnetic Bearings for Rotated Machines. Control and Experimants*. — Warsaw: Sci. Library of the Aviation Institute (in Polish).

Grega W. (1997): *Time-critical integrated control and design systems*. — Proc. Int. Conf. *Methods and Models in Automatics and Robotics*, Międzyzdroje, Poland, pp. 665–670.

Joo S. and Seo J.H. (1997): *Design and analysis of the nonlinear fedback linearizing control for a electromagnetic suspension system*. — IEEE Trans. Contr. Syst. Technol., Vol. 5, No. 1, pp. 135–144.

Kim M., Higuchi T., Mizuno T. and Hara H. (1998): *Application of a magnetic bearing spindle to non-circular fine boring*. — Proc. 6-th Int. Symp. *Magnetic Bearings*, Cambridge MA, pp. 22–31.

Lee A. and Fan Y. (1996): *Decentralized PID control of magnetic bearings in rotor system*. — Proc. 5-th Int. Symp. *Magnetic Bearings*, Kanazawa, Japan, pp. 13–18.

Levine J., Lottin J., and Ponsart J.C. (1996): *A nonlinear approach to the control of magnetic bearings*. — IEEE Trans. Contr. Syst. Technol., Vol. 4, No. 5, pp. 524–544.

Lin L.C. and Gau Y.-B. (1997): *Feedback linearization and fuzzy control for conical magnetic bearing*. — IEEE Trans. Contr. Syst. Technol., Vol. 5, No. 4, pp. 417–426.

Lottin J., Ponsart J.C. and Mouille P. (1996): *Non-linear control of active magnetic bearings. Digital implementation*. — Proc. 5-th Int. Symp. *Magnetic Bearings*, Kanazawa, Japan, pp. 77–82.

Math Works Inc. (1999): *Real–Time Windows Target User's Guide*. — Natick, MA: Math. Works Inc..

Mitkowski W. (1991): *Stabilization of Dynamical Control System*. — Warsaw: WNT, (in Polish).

Piłat A. (2002): *Feedback linearization control of AMB system*. — Proc. 8-th Int. Symp. *Magnetic Bearings* (ISMB-8), Mito, Japan, pp. 465–470.

Piłat A. (2002): *Control of magnetic levitation systems*. — Ph.D. Thesis, AGH-University of Science and Technology, Cracow, Poland.

Schweitzer G., Traxler A. and Bleuler H. (1993): *Magnetlager*. — Heidelberg: Springer.